**Conference paper**

Nandini Savoo, Frederick P. Malan, Lydia Rhyman and Ponnadurai Ramasami*

# Molecular insights of metal–metal interactions in transition metal complexes using computational methods

https://doi.org/10.1515/pac-2020-1212

**Abstract:** Computational methods were used to analyse the interactions around the metal centres in three transition metal (TM) complexes for which the X-ray data are available. We were particularly interested in understanding the metal–metal interactions. We used concepts of bond order, natural population, quantum theory of atom in molecules, electron localisation functions (ELFs) and non-covalent interactions (NCIs). Our results indicate that these tools can be used effectively to help in having insights into the bonding of TM complexes.

**Keywords:** Bond; chemistry and its applications ELF; NBO; NCI; QTAIM; VCCA-2020.

## Introduction

In 1916, Lewis proposed the chemical bond as a line representing a pair of electrons shared between two atoms [1]. However, this representation was based on chemical intuition rather than the laws of physics [2]. Heitler and London provided the first description of the chemical bond, which obeyed elementary physics; they employed quantum theory to describe interactions between two hydrogen atoms in the bonding and anti-bonding state of the hydrogen molecule [3]. However, Heitler and London's description of the chemical bond did not replace that of Lewis. Pauling bridged the gap between the two descriptions of the chemical bond through the valence bond (VB) theory [4]. The molecular orbital (MO) theory developed by Mulliken and Hund was much less accepted than the VB theory because delocalised MOs do not explain the localised chemical bond [5]. However, the MO theory successfully explains spectroscopic data and stability of aromatic compounds.

Although, to date, the line representation remains the basis of how chemists draw molecules and interpret reactions, much is still unknown about the chemical bond [2]. There is no well-established difference between the chemical and non-chemical interatomic interactions and this is the reason for the ongoing controversies about the chemical bond [2]. The chemical bond of main-group elements differs from that of transition metals. One major difference is that main-group elements make use of the *s* and *p* electrons in bonding whereas the

**Article note:** A collection of invited papers based on presentations at the Virtual Conference on Chemistry and its Applications (VCCA-2020) held on-line, 1–31 August 2020.

***Corresponding author: Ponnadurai Ramasami**, Computational Chemistry Group, Department of Chemistry, Faculty of Science, University of Mauritius, Réduit 80837, Mauritius; and Department of Chemical Sciences, University of Johannesburg, Doornfontein Campus, Johannesburg 2028, South Africa, e-mail: p.ramasami@uom.ac.mu
**Nandini Savoo,** Computational Chemistry Group, Department of Chemistry, Faculty of Science, University of Mauritius, Réduit 80837, Mauritius
**Frederick P. Malan,** Department of Chemistry, University of Pretoria, Hatfield, Pretoria 0002, South Africa
**Lydia Rhyman,** Computational Chemistry Group, Department of Chemistry, Faculty of Science, University of Mauritius, Réduit 80837, Mauritius; and Department of Chemical Sciences, University of Johannesburg, Doornfontein Campus, Johannesburg 2028, South Africa

© 2021 IUPAC & De Gruyter. This work is licensed under a Creative Commons Attribution-NonCommercial-NoDerivatives 4.0 International License. For more information, please visit: http://creativecommons.org/licenses/by-nc-nd/4.0/

bonding in transition metal (TM) complexes is best described by the *s* and *d* orbitals [2, 6]. This description of the chemical bond gave rise to the 18-electron rule [2].

The 18-electron rule is referred to as a way to make an initial guess about the presence of a bond [7]. The 18-electron rule correctly describes complexes with terminal ligands, such as $(CO)_nMM(CO)_n$. However, complexes with bridging ligands prove to be more complicated [8]; for instance, six different bonding descriptions are available for the $Os_3(CO)_{10}(\mu_2\text{-}H)_2$ complex are available in literature with the Os–Os bond orders varying from zero to two [8–11]. Moreover, in molecules with bridging hydrogen atoms, the 3-centre-2-electron (M($\mu$-H)M) interaction may be represented in different ways, leading to varying and debatable electron counts and bond orders [7].

A metal–metal interaction is expected when the interatomic distance is shorter than the sum of the van der Waals radii of the two metal atoms [12]. While this proximity of metal atoms may be considered as a metal–metal bond, this is not the scientific way of determining the presence of such a bond [7, 12–14]. Cotton and co-workers broached this matter by synthesising the $M_2(p\text{-}CH_3C_6H_4NCHNC_6H_4\text{-}p\text{-}CH_3)_2$ [M = Cu(I) and Ag(I)] complexes; X-ray crystallography displayed short M–M distances [13]. The authors optimised a model of the complex ($M_2(HNCHNH)_2$) using the SCF-Xα-SW method and performed MO calculations. They deduced that direct metal–metal bonds were not present in the complexes [13]. Cui et al. reported that the $Be_2B_8$ and $Be_2B_7^-$ complexes exhibit the shortest Be–Be interatomic distances (1.910 and 1.901 Å, respectively) [14]. However, these short interatomic distances do not translate to the presence of a Be–Be bond due to absence of valence electrons in the two Be atoms: the quantum theory of atoms in molecules (QTAIM) analysis shows no bond critical point and no bond path between the two Be atoms [14].

TM complexes have been extensively studied both experimentally and theoretically [15–19]. One of the experimental methods to determine the geometry, electron density distribution and the chemical bonding of a compound is the X-ray crystallography [15, 20]. However, when extended to organometallic complexes with heavy atoms, X-ray crystallography may be subject to limitations [15], for instance, the positions of the Co and Rh metals were not distinguishable in a TM complex [21]. Computational methods available for the characterisation of TM complexes are the bond order [22], natural bond orbital (NBO) population [23, 24] and topological analyses [12], among others.

The aim of this manuscript was to use computational methods to have insights into the interactions around the metal centres in three TM complexes for which the crystallographic information files (CIF) are available. In particular, we were interested in the metal–metal interactions in these complexes. Figure 1 shows the TM complexes. Gross et al. reported that the X-ray crystal structure of osmium(III) pentamethylcyclopentadienyl (**$TM_1$**) displays an Os–Os single metal bond, two bridging and two terminal bromide ligands [25]. **$TM_2$** is a monomer of the *p*-cymene-osmium which was obtained in a dimeric state with two bridging and one terminal Br ligands and no Os–Os interaction [26]. The $\mu$-chloro-$\mu$-hydrido-bis[chloro($\eta^6$-*p*-cymene)-ruthenium(II)] (**$TM_3$**) was reported to consist of one terminal and one bridging Cl ligands and an Ru–Ru bond [27].

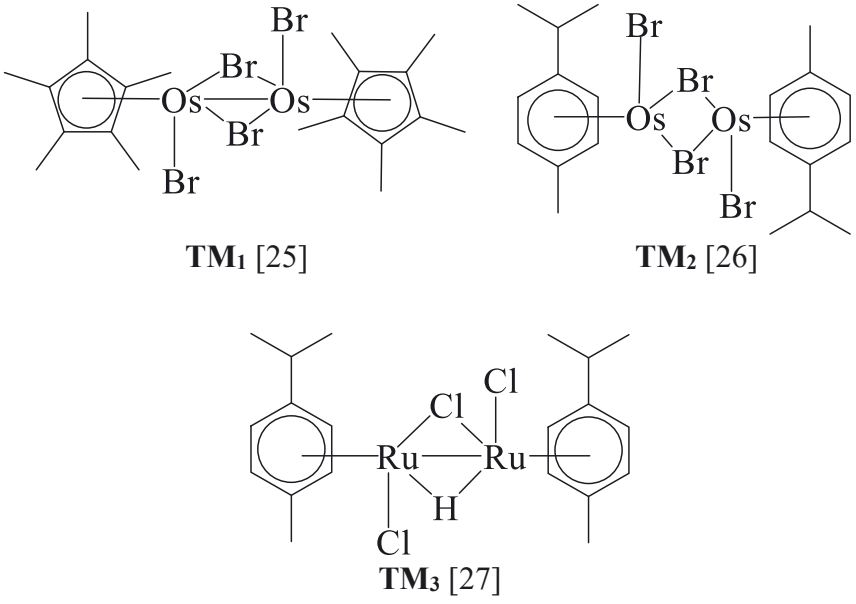


**$TM_1$** [25] **$TM_2$** [26] **$TM_3$** [27]

**Fig. 1:** TM complexes studied in this manuscript.

## Computational methods

The CIFs of the **$TM_1$**, **$TM_2$** and **$TM_3$** complexes were obtained from the Cambridge Crystallographic Data Centre (CCDC, May 2019 version). The Mercury 3.7 package [28–32] was employed to extract the crystallographic parameters of the complexes. The B3LYP [33–35] functional integrated in the Gaussian 16 suite [36] available on SEAGrid [37–41] was employed for all computations. A geometry optimisation of the crystallographic coordinates was performed with the LANL2DZ [42–45] relativistic effective core potential for the TM atoms (Ru and Os) and the 6-31G(d,p) basis set for the other atoms (C, H, Cl and Br). The LANL2DZ basis set has been used to analyse TM complexes in previous reports [18, 46]. No symmetry constraint was imposed. The electron count method was employed to predict the presence of metal–metal bonds in the organometallic complexes. The Multiwfn program [47] was employed to determine the Mayer, Fuzzy and Wiberg bond orders. We performed natural population analyses for the optimised geometries using NBO Version 3.1 [48, 49]. QTAIM analyses were performed using the AIMAll Version 17.11.14 software [50]. Electron localisation function (ELF) and non-covalent interaction (NCI) analyses were also performed using the Multiwfn software. The Visual Molecular Dynamics program [51], the Gnuplot 4.2 program [52] and Ghostscript interpreter [53] were employed to facilitate the NCI analyses. Visualisation software employed were CylView [54], GaussView 6.0 [55] and Chemcraft [56].

## Results and discussion

Figure 2 depicts the optimised geometries of the TM complexes. The substituents of the rings surrounding the metal (M) atoms have been faded.

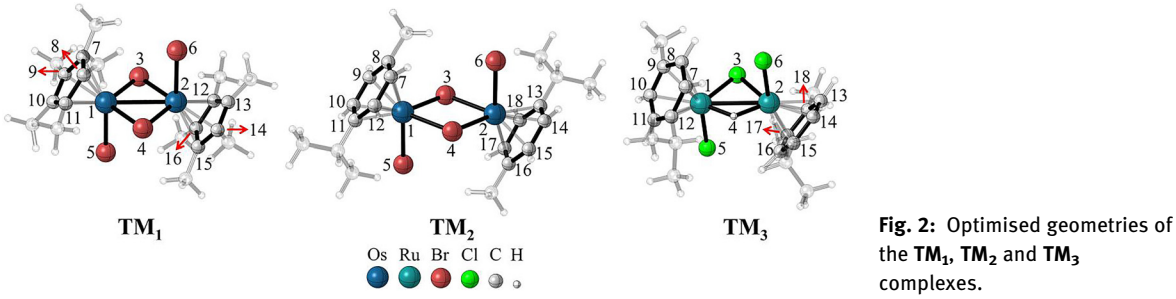


**Fig. 2:** Optimised geometries of the **$TM_1$**, **$TM_2$** and **$TM_3$** complexes.

### Structural parameters

Table 1 gives a comparison of the M–M bond distances of the optimised TM complexes with those of the X-ray crystal structures [25–27]. A complete list of bond lengths and bond angles is provided in the Supplementary Material (SM) file. The RMSD of all bond lengths and bond angles of the TM complexes are included in Table 1. The bond lengths of the optimised structures are longer than those in X-ray structures because the optimised structures are in gas phase whereas the X-ray structures are in the solid state [57]. This phenomenon is attributed to structural breathing in complexes [58].

**Table 1:** A comparison of the M–M bond distances in Å and the RMSD of the bond lengths in Å and bond angles in °.

| Complex | M–M bond distance/Å | | RMSD | |
|---|---|---|---|---|
| | Optimised | X-ray | Bond distances/Å | Bond angles/° |
| **$TM_1$** | 3.0327 | 2.9873 [25] | 0.0305 | 0.8 |
| **$TM_2$** | 4.0111 | 3.9006 [26] | 0.0453 | 3.6 |
| **$TM_3$** | 2.9904 | 2.9572 [27] | 0.0948 | 3.0 |

## Electron count methods

In general, a stable organometallic complex satisfies the 18-electron rule. The metal atom must possess a total of 18 electrons in its valence shell [2, 59]. With an electron configuration of [Xe]$6s^2 4f^{14} 5d^6$ for the Os atom and [Kr]$4d^7 5s^1$ for the Ru atom, either the covalent or ionic methods may be used to count the number of valence electrons. According to the electron count method, the presence of an M–M bond is required for **$TM_1$** and **$TM_3$** to satisfy the 18-electron rule. In the **$TM_2$**, however, the 18-electron rule is satisfied without the M–M bond (Fig. S1).

## Bond order

The Mayer, Fuzzy and Wiberg bond orders (Table 2) were obtained using the Multiwfn software. All three bond orders indicate the presence of an M–M bond only in **$TM_1$** and **$TM_3$**. The Wiberg bond order was decomposed into the contributions from the natural atomic orbital (NAO) pairs of the M atoms. Tables S7–S9 show the Wiberg bond orders and their decomposition analysis of M–A (A is the atom bonded to the TM M) bonds. The bond orders in Table 2 show the significant σ-bonding character between the 5*d* orbitals of Os1 and Os2 atoms in **$TM_1$**, no Os1–Os2 bonding in **$TM_2$** and weak σ-bonding between the 4*d* orbitals of Ru1 and Ru2 atoms.

**Table 2:** Mayer, Fuzzy and Wiberg bond orders and the Wiberg bond order decomposition analysis.

| Complex | M–M bond orders | | | Wiberg bond order decomposition analysis | |
|---|---|---|---|---|---|
| | Mayer | Fuzzy | Wiberg | Contribution | NAO type |
| **$TM_1$** | 0.5590 | 0.7619 | 0.5276 | 0.3676 | 5*d* (Os1) – 5*d* (Os2) |
| **$TM_2$** | – | 0.0979 | 0.0255 | [a] | – |
| **$TM_3$** | 0.2236 | 0.5110 | 0.2580 | 0.1175 | 4*d* (Ru1) – 4*d* (Ru2) |

[a]No contribution is detected from the M atoms.

## Frontier molecular orbital analyses

The frontier molecular orbital (FMO) was developed in the 1950s by Fukui [60]. The FMO is a description of the chemical reactivity and stability. The highest occupied molecular orbital (HOMO) represents the electron-donating ability of the complex while the lowest unoccupied molecular orbital (LUMO) is the ability to accept an electron [18]. HOMO and LUMO factors are of fundamental importance in understanding the chemical stability and reactivity of both organic and inorganic molecules [61]. Figure 3 shows the HOMO and LUMO of the TM complexes.

The HOMO of **$TM_1$**, **$TM_2$** and **$TM_3$** are –4.96, –5.44 and –5.39 eV, respectively. The contributions to the HOMO of **$TM_1$** are from the $d_{xy}$ orbitals on the Os atoms. The $p_z$ orbitals on terminal Br atoms and the $d_z^2$ and $d_{xz}$ orbitals on the Os atoms contribute to the HOMO of **$TM_2$**. Moreover, the HOMO of **$TM_3$** is made up of the $d_{xz}$ orbitals on Ru atoms and the $p_y$ orbitals on neighbouring C atoms.

The LUMO of **$TM_1$**, **$TM_2$** and **$TM_3$** are –3.10, –1.58 and –2.29 eV, respectively. The main contributions of the LUMO of **$TM_1$** are the $d_z^2$ orbitals on Os atoms, the $p_x$ orbitals on bridging Br atoms and the *s* orbitals on neighbouring C atoms. As for the LUMO of **$TM_2$**, the main contributions come from the *d* orbitals of the Os atoms. Furthermore, the main contributions to the LUMO of **$TM_3$** are the $d_{xy}$ orbitals on the Ru atoms and the $d_{x^2-y^2}$ orbital on Ru1.

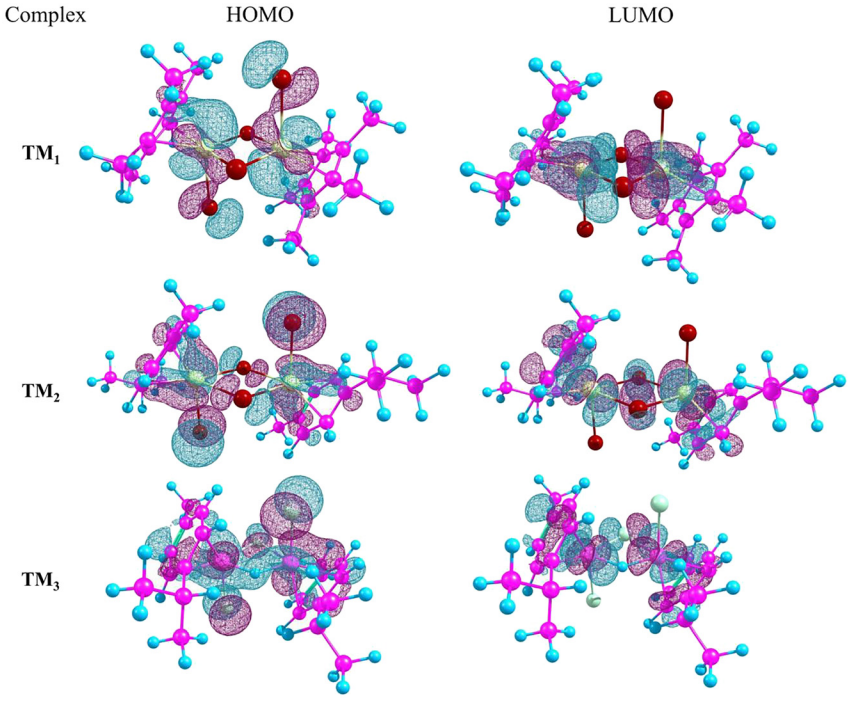


**Fig. 3:** HOMO and LUMO of the TM complexes.

## Natural population analysis

Table 3 shows the NBO analysis of the **$TM_1$** complex. M and A are the extent of polarisation of the M–A bond and the hybridisation of the orbital on the M or A atoms; A is the atom bonded to the TM M. %*s*, %*p* and %*d* represent the extent of hybridisation of the M–A bond at the M or A atoms. The s character for the M atom is higher in the M–Cl bond than in the M–C bond, which is the opposite of what was observed from main group chemistry [62, 63]. The same observation is made from the NBO analyses of **$TM_2$** and **$TM_3$** (Tables S13 and S14). The M–M bond is not detected by the NBO program in any of the TM complexes.

We also report the donor-acceptor interactions that involve the NBOs of the TM complexes (Table 4) from the second order perturbation theory analysis. The LP*4(Os2) NBO of **$TM_1$** shows considerable interaction (27.8 kcal $mol^{-1}$) with the LP*3(Os1); this indicates the presence of the Os1–Os2 bond. No such interaction is found between the NBOs of **$TM_2$** which indicates the absence of an Os–Os bond. In **$TM_3$**, several interactions are observed between the NBOs of Ru1 and Ru2 (Table 4). However, none are as strong as in **$TM_1$**.

**Table 3:** NBO analysis of the **$TM_1$** complex.

| Bond | M[a] | %*s*(M) | %*p*(M) | %*d*(M) | A[a] | %*s*(A) | %*p*(A) | %*d*(A) | Occupancy |
|---|---|---|---|---|---|---|---|---|---|
| Os1–Br3 | 29.6% $sp^{4.44}d^{6.24}$ | 8.6 | 38.0 | 53.4 | 70.4% $sp^{9.67}$ | 9.4 | 90.5 | 0.1 | 1.90 |
| Os1–Br3 | 17.3% $sp^{1.37}d^{2.35}$ | 21.2 | 29.0 | 49.9 | 82.7% $sp^{3.12}$ | 24.3 | 75.6 | 0.1 | 1.58 |
| Os1–Br5 | 25.2% $sp^{3.54}d^{1.64}$ | 16.2 | 57.3 | 26.6 | 74.8% $sp^{3.99}$ | 20.0 | 79.8 | 0.2 | 1.89 |
| Os1–C7 | 39.6% $sp^{11.72}d^{20.14}$ | 3.0 | 35.7 | 61.3 | 60.4% $sp^{20.94}$ | 4.6 | 95.4 | 0.1 | 1.38 |
| Os1–C8 | 43.7% $sp^{75.88}d^{99.99}$ | 0.4 | 28.1 | 71.5 | 56.3% $sp^{20.94}$ | 4.6 | 95.4 | 0.1 | 1.42 |
| Os1–Br4 | 26.8% $sp^{2.19}d^{1.94}$ | 19.5 | 42.7 | 37.8 | 73.2% $sp^{4.85}$ | 17.1 | 82.8 | 0.1 | 1.87 |
| Os2–Br4 | 27.6% $sp^{4.16}d^{3.78}$ | 11.2 | 46.5 | 42.3 | 72.5% $sp^{4.85}$ | 17.1 | 82.8 | 0.1 | 1.88 |
| Os2–Br6 | 28.8% $sp^{0.87}d^{1.51}$ | 29.6 | 25.8 | 44.6 | 71.2% $sp^{3.99}$ | 20.0 | 79.8 | 0.2 | 1.95 |
| Os2–C14 | 45.8% $sp^{0.83}d^{4.88}$ | 14.9 | 12.4 | 72.7 | 54.2% $sp^{20.81}$ | 4.6 | 95.3 | 0.1 | 1.45 |
| Os2–C13 | 60.2% $sp^{1.21}d^{15.17}$ | 5.8 | 6.9 | 87.3 | 39.8% $sp^{27.18}$ | 3.6 | 96.4 | 0.1 | 1.49 |
| Os2–C12 | 36.3% $sp^{5.37}d^{5.93}$ | 8.1 | 43.7 | 48.2 | 63.7% $sp^{95.34}$ | 4.6 | 95.3 | 0.1 | 1.38 |

[a]Percentage of polarisation of the M–A bond and hybridisation of the orbital on the M or A atoms.

**Table 4:** Second order perturbation theory analysis of the donor-acceptor interactions in the TM complexes.

| Donor NBO | Acceptor NBO | Interaction energy/kcal mol$^{-1}$ |
|---|---|---|
| **$TM_1$** | | |
| LP*4(Os2) | LP*3(Os1) | 27.8 |
| **$TM_3$** | | |
| LP*4(Ru1) | LP*6(Ru2) | 9.4 |
| LP*5(Ru1) | LP*6(Ru2) | 1.5 |
| LP*5(Ru1) | LP*6(Ru2) | 9.7 |

## QTAIM analysis

The QTAIM approach was employed to determine the covalent character of the M–M interactions. Figure 4 shows regions of minimum electron density called the bond critical points ($r_b$) and the ring critical points ($r_r$) in the **$TM_1$** complex in the QTAIM analysis. The electron density maps of the **$TM_2$** and **$TM_3$** complexes are shown in Figs. S2 and S3 in the SM. The lines in black are the bond paths, which have the maximum electron density [$\rho(r_b)$] between two chemically-bonded atoms. Table 5 lists the topological descriptors, such as the Laplacian of the electron density [$\nabla^2\rho(r)$], the distances ($d_1$ and $d_2$) of the $r_b$ and $r_r$ from the nuclei of the M1 and M2 atoms, the perpendicular and parallel curvatures at the $r_b$ ($\lambda_1$, $\lambda_2$ and $\lambda_3$), the electron delocalisation index [$\delta(M_1,M_2)$] and the total energy density [$H(r_b)$].

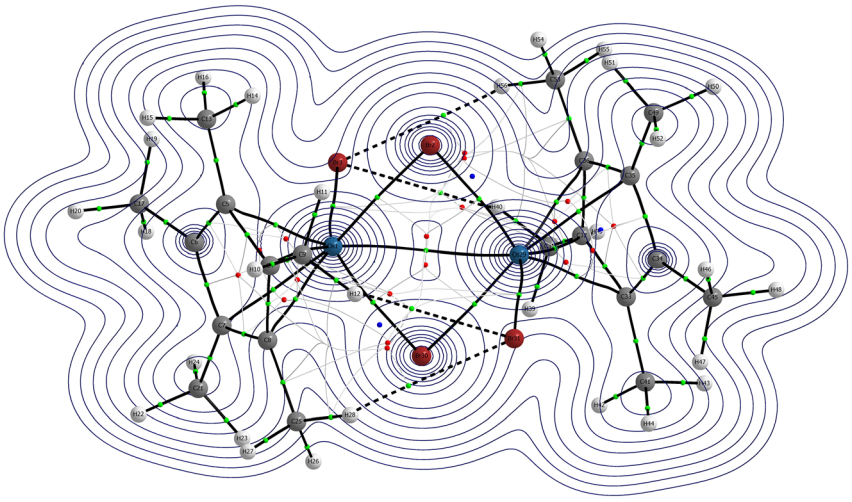

**Fig. 4:** Electron density map of the **$TM_1$** complex. The $r_b$ and $r_r$ are in green and red, respectively.

**Table 5:** Topological properties and QTAIM properties (in a.u.) at the $r_b$ in the TM complexes.

| Complex | $d_1$[a] | $d_2$[a] | $\rho(r_b)$ | $\nabla^2\rho(r_b)$ | $\lambda_1$ | $\lambda_2$ | $\lambda_3$ | $\lvert\lambda_1\rvert/\lambda_3$ | $\delta(M_1,M_2)$ | $H(r_b)$ |
|---|---|---|---|---|---|---|---|---|---|---|
| **$TM_1$** | 1.530 | 1.530 | 0.03520 | 0.03805 | −0.0168 | −0.0077 | 0.0625 | 0.2688 | 0.5253 | −0.0061 |
| **$TM_2$** | 2.011 | 2.011 | 0.01731 | 0.05324 | −0.0101 | 0.0102 | 0.0532 | 0.1898 | 0.0293 | 0.0013 |
| **$TM_3$** | 1.542 | 1.542 | 0.03332 | 0.07494 | −0.0206 | 0.0409 | 0.0547 | 0.5037 | 0.2352 | −0.0032 |

[a]$d_1$ and $d_2$ are the distances of the $r_b$ and $r_r$ to the metal nuclei in Å.

The $\rho(r_b)$, $\nabla^2\rho(r)$ and $|\lambda_1|/\lambda_3$ values are used to characterise the M–M interactions in the TM complexes [64]. The $\rho(r_b)$, $\nabla^2\rho(r)$ and $|\lambda_1|/\lambda_3$ values of the TM complexes are small, greater than zero and less than one, respectively. This implies a typical closed-shell (electrostatic) interaction between the M atoms [64]. However, the negative $H(r_b)$ values show that the M–M bonds in **$TM_1$** and **$TM_3$** have covalent character. The covalent character of the M–M bond in **$TM_3$** is lower as the $H(r_b)$ is lower than that of **$TM_1$**. Although low $\delta(M_1,M_2)$ values are associated with M–M bonds, the near-zero $\delta(M_1,M_2)$ for the **$TM_2$** complex shows that no M–M bonding occurs.

## Electron localisation functions

We performed a topological analysis of the ELF of the electronic structures of the TM complexes whereby these structures are described by local maxima (attractors) and localisation domains of the ELF. The attractors and localisation domains characterise core regions, lone pairs of electrons and valence regions. The points, by which a steepest ascent leads to the attractor, form the basin of the attractor. Two types of basins are observed in a molecule: core and valence. The valence basins may be monosynaptic or polysynaptic, which correspond to a lone pair of electrons or a many-centre bond [65]. An integration of the basin gives the electron population of the basin.

Figure 5 shows the ELF attractors and the localisation domains of the TM complexes. Table 6 lists the electron population to which the selected disynaptic basins integrate and the ELF values of the attractors. In **$TM_1$**, the attractors along the Os–Br bonds are located closer to the Br atom (Fig. 5a), which reflects the higher electronegativity of the Br atom. This is shown by the localisation domain (orange) with ELF value of 0.77 (Table 6) located closer to the Br atom and in the direction of the Os atom (Fig. 5b). From the ELF basin analysis of the **$TM_1$** complex, it is observed that the disynaptic basins of the bridging ligands [V(Os1,Br3), V(Os2,Br3), V(Os2,Br4) and V(Os2,Br4)] have a higher electron population (0.75 e) than those of the terminal ligands (V(Os1,Br5) and V(Os2,Br6); 0.60 e).The attractor for the Os1–Os2 bond is located in the middle of the bond

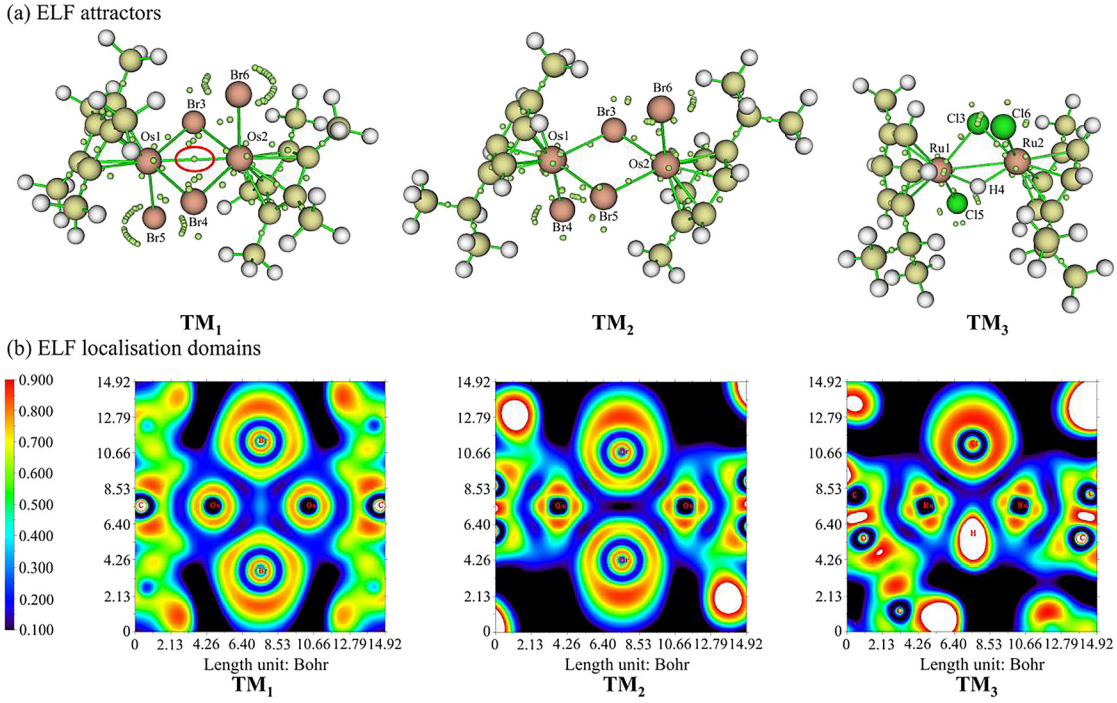


**Fig. 5:** (a) ELF localisation domains and (b) ELF attractors of the TM complexes. The attractor between the Os atoms in **$TM_1$** is encircled in red.

**Table 6:** The electron population of selected basins (attractors shown in Fig. 6). M and A can be understood from Fig. 5.

| Basin | Electron population | | | ELF value | | |
|---|---|---|---|---|---|---|
| | $TM_1$ | $TM_2$ | $TM_3$ | $TM_1$ | $TM_2$ | $TM_3$ |
| V(M1,M2) | 0.15 | – | – | 0.327 | – | – |
| V(M1,A3) | 0.75 | 0.95 | 0.68 | 0.777 | 0.801 | 0.860 |
| V(M2,A3) | 0.75 | 0.96 | 0.68 | 0.777 | 0.802 | 0.860 |
| V(M1,A4) | 0.75 | 0.96 | 1.66 | 0.777 | 0.802 | 1.000 |
| V(M2,A4) | 0.75 | 0.95 | 1.66 | 0.777 | 0.801 | 1.000 |
| V(M1,A5) | 0.60 | 0.55 | 0.49 | 0.777 | 0.763 | 0.834 |
| V(M1,A6) | 0.60 | 0.55 | 0.49 | 0.777 | 0.763 | 0.834 |

(encircled in red in Fig. 5) with an ELF value of 0.33 and a V(Os1,Os2) disynaptic basin with 0.15 e. Similar observations are made for the bridging and terminal ligands of $\mathbf{TM_2}$ and $\mathbf{TM_3}$. The two differences are: (i) No attractor is located between the M atoms of $\mathbf{TM_2}$ and $\mathbf{TM_3}$ and (ii) the V(Ru1,H4) and V(Ru2,H4) protonated attractors are localised at the core of the H atom with an electron population of 1.66 e and an ELF value of 1.00. Although the bond order and NBO analyses indicate the presence of an Ru–Ru bond in $\mathbf{TM_3}$, no attractor was observed between the Ru atoms due to the lower covalent character of the Ru–Ru interaction as determined by the QTAIM analysis.

## Non-covalent interactions

We also performed an NCI analysis of the TM complexes. The NCI plots generated allow for a visualisation of NCIs between molecular fragments as real-space surfaces. Within the NCI framework, the sign of $\lambda_2$ enables identification of the interaction type. Attractive interactions are negative, van der Waals interactions occur close to zero and steric repulsions are positive.

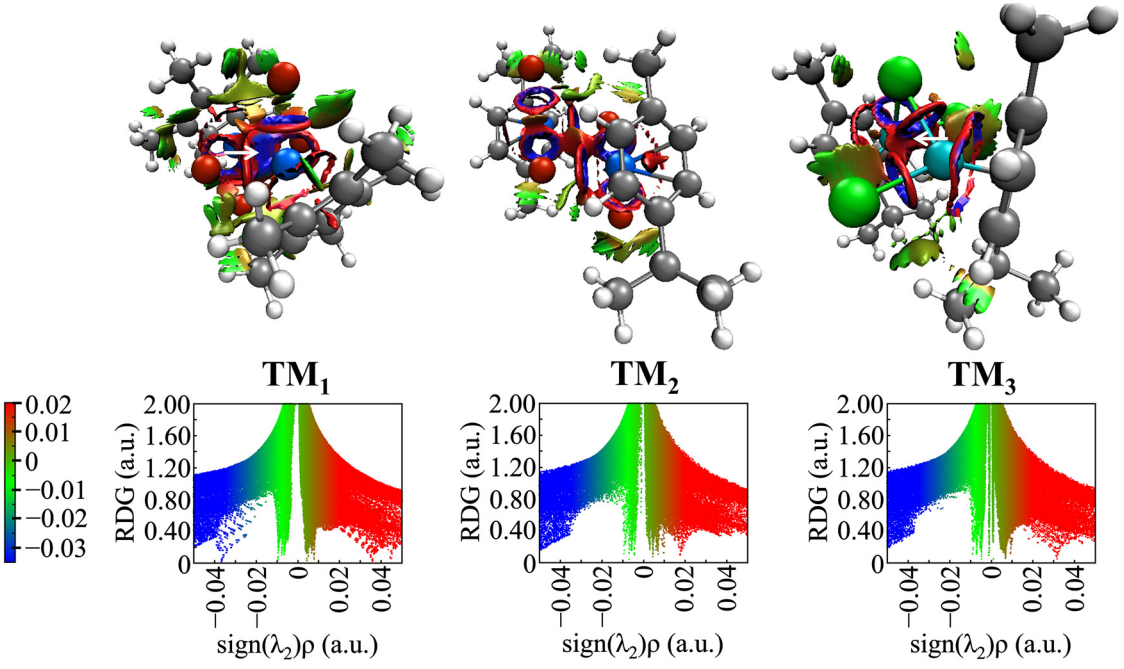


**Fig. 6:** 2D and 3D NCI plots of the TM complexes. The NCI isosurfaces correspond to an isovalue of s = 0.5 a.u.

The NCI isosurfaces in Fig. 6 correspond to an isovalue of s = 0.5 a.u. In the 3D plot for the **$TM_1$** complex, a blue patch between the two Os atoms indicates an attractive NCI which produces a spike at almost sign($\lambda_2$)ρ = –0.04 a.u. Green isosurfaces representing van der Waals forces of attraction are present between the Br atoms and the H atoms of the neighbouring methyl groups. These van der Waals forces of attraction span over the 0 > sign($\lambda_2$)ρ > –0.01. Between the Os and Br atoms and the Os and C atoms, an attractive isosurface is observed which is enclosed by a repulsive wall at around sign($\lambda_2$)ρ = 0.035 a.u. The non-bonded overlap between the C atoms of the phenyl rings neighbouring the Os atoms causes a steric repulsion shown by the red region in the 2D plot. The NCI plots for the **$TM_2$** and **$TM_3$** complexes show similar isosurfaces. However, no spike is observed in the attractive region of the 2D plot of the **$TM_2$** and **$TM_3$** complexes. Instead, a trough at approximately sign($\lambda_2$)ρ = 0.01 a.u. is observed in the 2D plot of the **$TM_2$** complex, which is represented by a brown isosurface in the 3D plot. This is due to steric repulsion which arises due to the Os1–Br3–Os2–Br4 ring. The same is observed for the **$TM_3$** complex at around sign($\lambda_2$)ρ = 0.03 a.u.

## Conclusions

Computational methods were employed to gain insights into interactions in three TM complexes for which CIFs are available. The methods of analysis employed were bond orders, NBO, QTAIM, ELF and NCI. The bond order and NBO analyses indicate the presence of an M–M bond in **$TM_1$** and **$TM_3$** but not in **$TM_2$**. The M–M bond in **$TM_3$** appears weaker than that in **$TM_1$**. The M–M bond in **$TM_1$** was found to be electrostatic with some covalent character by the QTAIM analyses. The ELF analysis confirms a two-centre bond between the Os atoms in **$TM_1$** with an electron population of 0.15 e. Moreover, an attractive isosurface exists between the Os atoms in **$TM_1$**, which was deduced by the NCI analysis. As for the **$TM_2$** complex, no bond path, no attractor and a repulsive isosurface were observed between the Os atoms, which imply the absence of an M–M bond in **$TM_2$**. The QTAIM analysis of **$TM_3$** indicates that the M–M bond is electrostatic with lower covalent character than in the **$TM_1$** complex. This translates to the absence of an attractor and the presence of a repulsive surface between the Ru atoms. We hope that this manuscript strengthens the idea of using computational methods to complement X-ray data.

**Acknowledgments:** Mr S De Beer is acknowledged for help with QTAIM and helpful discussions.
**Research funding:** We are thankful to the Higher Education Commission (HEC) of Mauritius for financial support and to SEAGrid for computing facilities. This work has received support from the South African National Research Foundation (FPM: Grant number 117995) which is gratefully acknowledged.

## References

[1] G. N. Lewis. *J. Am. Chem. Soc.* **38**, 762 (1916).
[2] F. Gernot, S. Sason. *The Chemical Bond*, WILEY-VCH Verlag GmbH & Co., Germany (2014).
[3] W. Heitler, F. London. *Z. Phys.* **44**, 455 (1927).
[4] L. Pauling. *The Nature of the Chemical Bond*, Cornell University Press, New York (1939).
[5] A. Simões, K. Gavroglu. in *Conceptual Perspectives in Quantum Chemistry*, J.-L. Calais, E. Kryachko (Eds.), pp. 383–413, Springer, Dordrecht (1997).
[6] C. R. Landis, T. K. Firman, D. M. Root, T. Cleveland. *J. Am. Chem. Soc.* **120**, 1842 (1998).
[7] G. Parkin. in *Structure and Bonding*, D. M. Mingos (Ed.), pp. 561–563, Springer, Berlin, Heidelberg (2010).
[8] M.-H. Baik, R. A. Friesner, G. Parkin. *Polyhedron* **23**, 2879 (2004).
[9] V. F. Allen, R. Mason, P. B. Hitchcock. *J. Organomet. Chem.* **140**, 297 (1977).
[10] M. R. Churchill, F. J. Hollander. J. P. Hutchinson. *Inorg. Chem.* **16**, 2697 (1977).
[11] A. G. Orpen, A. V. Rivera, E. G. Bryan, D. Pippard, G. M. Sheldrick, K. D. Rouse. *J. Chem. Soc., Chem. Commun.* **723** (1978).
[12] C. Lepetit, P. Fau, K. Fajerwerg, M. L. Kahn, B. Silvi. *Coord. Chem. Rev.* **345**, 150 (2017).

[13] F. A. Cotton, X. Feng, M. Matusz, R. Poli. *J. Am. Chem. Soc.* **110**, 7077 (1988).
[14] Z. Cui, W. Yang, L. Zhao, Y. Ding, G. Frenking. *Angew. Chem.* **128**, 7972 (2016).
[15] P. Macchi, A. Sironi. *Coord. Chem. Rev.* **238–239**, 383 (2003).
[16] W. Liang, D. Li, P.-L. Lau, L. Xu, C. Yang, M. Wei, W. T.-K. Chan, W.-Y. Wong. *J. Organomet. Chem.* **870**, 8 (2018).
[17] M. Imran, Zia-ur-Rehman, T. Kondratyuk, F. Bélanger-Gariepy. *Inorg. Chem. Commun.* **103**, 12 (2019).
[18] Y. Sert, H. S. Clayton, H. Gökce, K. C. Tapala. *J. Mol. Struct.* **1188**, 86 (2019).
[19] S. A. Al-Jibori, L. A. Al-Doori, A. S. M. Al-Janabi, M. A. Alheety, H. Akbaş, A. Karadag. *J. Mol. Struct.* **1207**, 127832 (2020).
[20] S. Galli. *J. Chem. Educ.* **91**, 2009 (2014).
[21] M. C. Cheng, C. L. Mai, C. Y. Yeh, G. H. Lee, S. M. Peng. *Chem. Commun.* **49**, 7938 (2013).
[22] J. F. Berry. in *Structure and Bonding*, G. Parkin (Ed.), pp. 1–28, Springer Berlin Heidelberg, Berlin, Heidelberg (2010).
[23] F. Weinhold, C. R. Landis. *Discovering Chemistry with Natural Bond Orbitals*, John Wiley & Sons, Hoboken, New Jersey (2012).
[24] F. Weinhold, C. R. Landis, E. D. Glendening. *Int. Rev. Phys. Chem.* **35**, 399 (2016).
[25] C. L. Gross, J. L. Brumaghim, G. S. Girolami. *Organometallics* **26**, 2258 (2007).
[26] H. S. Clayton, B. C. E. Makhubela, H. Su, G. S. Smith, J. R. Moss. *Polyhedron* **28**, 1511 (2009).
[27] B. Therrien, S. Frein, G. Süss-Fink. *Acta Crystallogr. E* **60**, 1666 (2004).
[28] C. F. Macrae, I. J. Bruno, J. A. Chisholm, P. R. Edgington, P. McCabe, E. Pidcock, L. Rodriguez-Monge, R. Taylor, J. van de Streek, P. A. Wood. *J. Appl. Crystallogr.* **41**, 466 (2008).
[29] C. F. Macrae, P. R. Edgington, P. McCabe, E. Pidcock, G. P. Shields, R. Taylor, M. Towler, J. van de Streek. *J. Appl. Crystallogr.* **39**, 453 (2006).
[30] I. J. Bruno, J. C. Cole, P. R. Edgington, M. K. Kessler, C. F. Macrae, P. McCabe, J. Pearson, R. Taylor. *Acta Crystallogr*. **B58**, 389 (2002).
[31] F. H. Allen, I. J. Bruno. *Acta Crystallogr.* **B66**, 380 (2010).
[32] R. Taylor, C. F. Macrae. *Acta Crystallogr*. **B57**, 815 (2001).
[33] A. D. Becke. *Phys. Rev.* **38**, 3098 (1988).
[34] C. Lee, W. Yang, R. G. Parr. *Phys. Rev. B* **37**, 785 (1988).
[35] B. Miehlich, A. Savin, H. Stoll, H. Preuss. *Chem. Phys. Lett.* **157**, 200 (1989).
[36] M. J. Frisch, G. W. Trucks, H. B. Schlegel, G. E. Scuseria, M. A. Robb, J. R. Cheeseman, G. Scalmani, V. Barone, G. A. Petersson, H. Nakatsuji, X. Li, M. Caricato, A. V. Marenich, J. Bloino, B. G. Janesko, R. Gomperts, B. Mennucci, H. P. Hratchian, J. V. Ortiz, A. F. Izmaylov, J. L. Sonnenberg, D. Williams-Young, F. Ding, F. Lipparini, F. Egidi, J. Goings, B. Peng, A. Petrone, T. Henderson, D. Ranasinghe, V. G. Zakrzewski, J. Gao, N. Rega, G. Zheng, W. Liang, M. Hada, M. Ehara, K. Toyota, R. Fukuda, J. Hasegawa, M. Ishida, T. Nakajima, Y. Honda, O. Kitao, H. Nakai, T. Vreven, K. Throssell, J. A. Montgomery, J. E. Peralta, F. Ogliaro, M. J. Bearpark, J. J. Heyd, E. N. Brothers, K. N. Kudin, V. N. Staroverov, T. Keith, R. Kobayashi, J. Normand, K. Raghavachari, A. P. Rendell, J. C. Burant, S. S. Iyengar, J. Tomasi, M. Cossi, J. M. Millam, M. Klene, C. Adamo, R. Cammi, J. W. Ochterski, R. L. Martin, K. Morokuma, O. Farkas, J. B. Foresman, D. J. Fox. *Gaussian 16, Version A.03*, Gaussian, Inc., Wallingford CT (2016).
[37] S. Pamidighantam, S. Nakandala, E. Abeysinghe, C. Wimalasena, S. Rathnayakae, S. Marru, M. Pierce. *Procedia Comput. Sci.* **80**, 1927 (2016).
[38] N. Shen, Y. Fan, S. Pamidighantam. *J. Comput. Sci.* **5**, 576 (2014).
[39] R. Dooley, K. Milfeld, C. Guiang, S. Pamidighantam, G. Allen. *J. Grid Comput.* **4**, 195 (2006).
[40] K. Milfeld, C. Guiang, S. Pamidighantam, J. Giuliani. *Cluster Computing through an Application-oriented Computational Chemistry Grid. Proceedings of the 2005 Linux Clusters: The HPC Revolution*, Linux Clusters Institute, New Mexico (2005).
[41] This work used the Extreme Science and Engineering Discovery Environment (XSEDE), which is supported by National Science Foundation grant number OCI-1053575.
[42] T. H. Dunning Jr., P. J. Hay. in *Modern Theoretical Chemistry*, H. F. Schaefer III (Ed.), pp. 1–28, Plenum, New York (1977).
[43] P. J. Hay, W. R. Wadt. *J. Chem. Phys.* **82**, 299 (1985).
[44] W. R. Wadt, P. J. Hay. *J. Chem. Phys.* **82**, 284 (1985).
[45] P. J. Hay, W. R. Wadt. *J. Chem. Phys.* **82**, 270 (1985).
[46] S. Taboukhat, N. Kichou, J.-L. Fillaut, O. Alévêque, K. Waszkowska, A. Zawadzka, A. El-Ghayoury, A. Migalska-Zalas, B. Sahraoui. *Sci. Rep.* **10**, 15292 (2020).
[47] T. Lu, F. Chen. *J. Comput. Chem.* **33**, 580 (2012).
[48] A. E. Reed, F. Weinhold. *J. Chem. Phys.* **78**, 4066 (1983).
[49] A. E. Reed, R. B. Weinstock, F. Weinhold. *J. Chem. Phys.* **83**, 735 (1985).
[50] AIMAll, Version 17.11.14. T. A. Keith, TK Gristmill Software, Overland Park KS, USA (2017), aim.tkgristmill.com.
[51] W. Humphrey, A. Dalke, K. Schulten. *J. Mol. Graph.* **14**, 33 (1996).
[52] T. Williams, C. Kelley. *Gnuplot 4.2: An interactive plotting program* (2007).
[53] Ghostscript, Version 9.53.3, www.artifex.com.
[54] CYLview 1.0b, C. Y. Legault. *Université de Sherbrooke* (2009), http://www.cylview.org/.

[55] R. Dennington, T. A. Keith, J. M. Millam. GaussView, Version 6, Semichem Inc., Shawnee Mission, KS (2016).
[56] G. A. Zhurko, D. A. Zhurko. ChemCraft, Version 1.7 (2013), http://www.chemcraftprog.com.
[57] W. J. Hehre. *A Guide to Molecular Mechanics and Quantum Chemical Calculations*, Wavefunction, Inc., USA (2003).
[58] J. Ponce-de-León, R. Infante, M. Pérez-Iglesias, P. Espinet. *Inorg. Chem.* **59**, 16599 (2020).
[59] P. B. Armentrout. *Science* **361**, 849 (2018).
[60] K. Fukui. *Science* **218**, 747 (1982).
[61] P. Shafieyoon, E. Mehdipour, Y. S. Mary. *J. Mol. Struct.* **1181**, 244 (2019).
[62] V. Jonas, C. Boehme, G. Frenking. *Inorg. Chem.* **35**, 2097 (1996).
[63] M. Kaupp. *Chem. Eur J.* **5**, 3631 (1999).
[64] E. Matito, J. Poater, F. M. Bickelhaupt, M. Solà. *J. Phys. Chem. B* **110**, 7189 (2006).
[65] Y. Grin, A. Savin, B. Silvi. *Chem. Bond* **345** (2014).

**Supplementary Material:** The online version of this article offers supplementary material (https://doi.org/10.1515/pac-2020-1212).